Research Square

Preprints are preliminary reports that have not undergone peer review. They should not be considered conclusive, used to inform clinical practice, or referenced by the media as validated information.

Metformin promotes the expansion of CD8+ central memory T cells by offsetting Pentose phosphate pathway

Xiao Feng Hong
Sun Yat-sen University
Hai Cheng Liu
Sun Yat-sen University
Shi Zhen Qing
The First Affiliated Hospital of Sun Yat-Sen University
Shao Qian Chen
The First Affiliated Hospital of Sun Yat-Sen University
Jian Yong Zou
The First Affiliated Hospital of Sun Yat-Sen University
Chuan Gang Lu
Sanya Central Hospital
Hua Run Yu
The First Affiliated Hospital of Sun Yat-Sen University
Jia Xuan Tan
Sun Yat-sen University
Yong Gu
The First Affiliated Hospital of Sun Yat-Sen University
Hai Hong
hongh3@mail.sysu.edu.cn

Sun Yat-sen University

Research Article

Keywords: Immunometabolism, Metformin, CD8+central memory T cell, Pentose phosphate pathway

Posted Date: October 15th, 2026

DOI: https://doi.org/10.21203/rs.3.rs-11117746/v1

License: This work is licensed under a Creative Commons Attribution 4.0 International License.
Read Full License

Additional Declarations: No competing interests reported.

Metformin promotes the expansion of CD8+ central memory T cells by offsetting Pentose phosphate pathway

Xiao Feng Hong[1*], Hai Cheng Liu[1,4*], Shi Zhen Qing[2*], Shao Qian Chen[3], Jian Yong Zou[2], Chuan Gang Lu[5], Hua Run Yu[2], Jia Xuan Tan[1], Yong Gu[2#],Hai Hong[1#]

1 Key Laboratory of Tropical Disease Control of Sun Yat-Sen University, Ministry of Education, The Institute of Immunology of Zhong Shan Medical School, Sun Yat-Sen University, Guangzhou, China, 2 Department of Thoracic Surgery, The First Affiliated Hospital of Sun Yat-Sen University, Guangzhou, China, 3 Department of Clinical Laboratory, The First Affiliated Hospital, Sun Yat-sen University, Guangzhou 4 Department of Clinical Laboratory, The Sixth Affiliated Hospital, Sun Yat-sen University, Guangzhou, China, 5 Department of Thoracic Surgery, Sanya Central Hospital, Sanya, China

*Co-first author

Co-corresponding author

Xiao Feng Hong, hongxf3@mail2.sysu.edu.cn

Hai Cheng Liu, liuhch59@mail.sysu.edu.cn

Shi Zhen Qing, qingshzh@mail2.sysu.edu.cn

Shao Qian Chen, chenshq28@sysu.edu.cn

Jian Yong Zou, zjyong@mail.sysu.edu.cn

Chuan Gang Lu, lcgsysu@163.com

Hua Run Yu, yuhr25@mail2.sysu.edu.cn

Jia Xuan Tan, tanjx28@mail2.sysu.edu.cn

Hai Hong, Key Laboratory of Tropical Disease Control of Sun Yat-sen University, Ministry of Education, The Institute of Immunology of Zhong Shan Medical School, Sun Yat-sen University, Guangzhou, China. Email: hongh3@mail.sysu.edu.cn

Yong Gu, Department of Thoracic Surgery, The First Affiliated Hospital of Sun Yat-sen University, Guangzhou, China. Email: guyong@mail.sysu.edu.cn

Abstract

$CD8^+$ central memory T (Tcm) cells underpin long-lived antitumor and antiviral immune responses, but their numbers wane with advancing age. Metformin promotes $CD8^+$ memory T-cell generation and tumor infiltration; however, its effect on the distribution of circulating $CD8^+$ memory subsets, especially $CD8^+$Tcm cells, has not been established. In this study, we isolated peripheral blood mononuclear cells (PBMCs) from middle-aged healthy donors (45–65 years) undergoing routine health screening. In vitro treatment with 20 mM metformin for 24 hours increased the frequency of $CD8^+$Tcm cells and promoted a metabolic shift characterized by enhanced expression of CPT1a, a rate-limiting enzyme of fatty acid oxidation (FAO), together with elevated ATP5a expression, increased mitochondrial mass and mitochondrial ROS (mtROS) production. Metformin also upregulated glucose-6-phosphate dehydrogenase (G6PD) while reducing the expression of glycolysis-associated enzymes HK1 and HK2. Collectively, these findings implicate the FAO–OXPHOS–ROS–PPP axis as a regulator of metformin-induced $CD8^+$ Tcm expansion and reveal the metabolic plasticity of human $CD8^+$ memory T cells during midlife.

This suggests that metabolic modulation may offer a strategy to support T-cell homeostasis across the ageing trajectory.

Key words: Immunometabolism, Metformin, CD8+central memory T cell, Pentose phosphate pathway

Introduction

Memory T cells (Tm cells) orchestrate adaptive immunity through coordinated cytokine secretion and cytotoxic granule-mediated killing, thereby controlling pathogen infections, eliminating neoplastic cells, and potentiating vaccine-induced immunological memory [1-2]. The heterogeneity of memory T cell subsets is characterized by distinct phenotypic markers, migratory patterns, and tissue-specific functions. Notably, CD8+memory T cells comprise two major populations: central memory T cells (Tcm), which exhibit lymphoid tropism through CCR7-mediated chemotaxis, demonstrat high proliferative capacity and self-renewal potential; effector memory T cells (Tem), prioritize effector functions by producing abundant cytokines. Ageing is accompanied by progressive remodeling of the T-cell compartment, including contraction of the naïve T-cell pool, accumulation of more differentiated memory populations, and alterations in T-cell homeostasis and metabolic regulation[3], our initial study found that the increased number of memory T cells was due to an increase in Tem cells, while the frequency of CD8+Tcm cells was at the low level across different age groups [4]. Compared to Tem cells, Tcm cells exhibit superior persistence and enhanced antitumor immunogenicity [5-6]. Therefore, understanding how CD8+ Tcm cells can be maintained or expanded during midlife may provide insight into preserving durable T-cell immunity across the ageing trajectory.

Metabolic reprogramming fundamentally governs T cell differentiation. Naïve T cells (Tn) exhibit quiescent metabolic features and mainly rely on oxidative phosphorylation (OXPHOS) for homeostatic proliferation and migration, and Tn cells preferentially utilize glucose. Upon activation, effector T cells undergo metabolic remodeling characterized by aerobic glycolysis upregulation, downregulate fatty acid oxidation (FAO) and enhanced fatty acid synthesis which is required for their expansion during the activation phase [7-8]. FAO has been observed in the generation and maintenance of long-lived memory CD8+T cells [9-12], OXPHOS also sustains memory T cell survival and energetic demands. Different memory T subsets possess distinct metabolic signatures. Tcm cells display high mitochondrial biogenesis and OXPHOS capacity, preferentially utilizing glucose-derived fatty acids through β-oxidation for ATP generation [13-15]; Tem cells utilize multiple substrates to fuel glycolysis and OXPHOS for supporting rapid effector functions [16-17].

Metformin (dimethylbiguanide) has become one of the first-line medication in the treatment of type II diabetes (T2D) since 1957. In recent years, multiple studies have shown that metformin has a favorable effect on the obesity, cancer, aging, neurodegeneration, cardiovascular disease [18-21]. Metformin treatment regulates the metabolism and differentiation of T cells; Metformin treatment enhanced CD8+memory T cell formation by modulating FAO [22-23]. Metformin produces mtROS to ensure CD8+TILs' proliferation via activation of the Nrf2/mTORC1/p62 axis in mice B16 melanoma model [24]. In multiple types of human cancer, taking metformin

contributes to anti-tumor effects by increasing the infiltration of CD8+T cells and decreasing Treg cells [25]. The metabolic reprogramming in T cell subsets from human PBMCs by treatment with metformin needs to be further explored.

However, how metformin reshapes T-cell metabolism during mid-age population, when age-associated alterations in immune homeostasis are already emerging but may remain metabolically modifiable, remains poorly understood. Therefore, we investigated the effects of metformin on memory T-cell differentiation and associated metabolic characteristics in PBMCs from middle-aged adults aged 45–65 years. In our study, we found that the frequency of human CD8+Tcm cells increased with metformin treatment; metformin enhanced the expression of CPT1a-a rate limiting enzyme of FAO in CD8+Tcm cells, and higher ATP5a, mitochondrial mass and mtROS production, increased glucose-6-phosphate dehydrogenase (G6PD), which may induce more glucose-6-phosphate (G6P) flowed into the pentose phosphate pathway (PPP), and we detected the decreased expression level of G6P. We also observed that metformin treatment reduced the expression of glycolysis-related key enzymes HK1 and HK2. This data revealed the FAO/OXPHOS/ROS/PPP axis as a regulator of metformin-induced human $CD8^+$Tcm expansion. Furthermore, our works revealed that basal and metformin modulates the metabolic spectrum of other T cell subsets, providing a foundation for better-recognized human T cell metabolism.

Results

The frequency of CD8+ central memory T cells increased with metformin treatment

Our prior work demonstrated that metformin attenuates T cell senescence and preserves undifferentiated T cell phenotypes in middle-aged individuals [4]. To further characterize its subset-specific immunomodulation, we performed phenotypic profiling in 138 healthy donors aged 44-65 years (mean ± SD, 53.59 ± 5.80; Table 1). CD4+ and CD8+ T cell subsets (Tn,Tcm, Tem, Teff) were gated based on CD45RA and CCR7 expression with standardized FMO controls (Fig.1a; Sup Fig.1a). Metformin induced a 2.15-fold expansion in CD8+Tcm frequency (9.42% vs 4.39%, $p<0.0001$; Fig.1b), accompanied by elevated absolute CD8+Tcm counts ($p=0.009$; Fig. 1c). Within CD8+T cells, metformin reduced Tn and Tem frequencies while increasing Teff abundance. In contrast, metformin decreased CD4+Tcm, Tn and Tem populations and expanded CD4+Teff cells, indicating distinct metformin-mediated regulation of CD4+ and CD8+T cell homeostasis (Fig.1e).

Increased fatty acid oxidation (FAO)across CD8+ T subsets cells with Metformin treatment

Memory T cell subsets exhibit intrinsic metabolic specialization: Tcm cells preferentially utilize FAO and OXPHOS, while Tem cells rely on glycolysis to sustain effector functions [26]. To characterize metformin-dependent FAO modulation, we examined CPT1a, the rate-limiting enzyme of FAO. Baseline CPT1a expression was uniformly high across CD8+T subsets, with comparable positivity in Tcm (Fig.2a), Tem (Fig.2c), Tn and Teff populations (Fig. 2e). Metformin significantly increased CPT1a+ frequencies in CD8+ Tem ($p=0.0013$, Fig.2c) and Teff cells ($p=0.0236$, Fig.2e) and elevated CPT1a MFI across all CD8+T compartments ($p=0.0155$, Fig.2b; $p=0.0002$, Fig.2d; $p=0.0148$, $p=0.0036$, Fig.2f). Relative to CD8+T cells, CD4+T cells displayed higher basal CPT1a levels (Sup.Fig.1b–e). Metformin selectively upregulated CPT1a in CD4+Tcm ($p=0.0252$, Sup Fig.1c) and Tn cells ($p=0.023$, Sup Fig.1e), with no significant changes in CD4+Tem and Teff subsets (Sup Fig.1d–e). These results indicate that metformin induces broad CPT1a upregulation in

CD8+T cells and exerts subset-specific FAO regulation in CD4+ T cells.

Metformin augments mitochondrial metabolic characteristics within subsets of CD8+ T cells.

Mitochondrial metabolism dictates T cell fate and function. Memory T cells exhibit enhanced mitochondrial respiration and preferentially employ FAO and OXPHOS to sustain long-term survival and rapid recall responses compared with terminally differentiated effector T cells [9]. Although metformin remodels mitochondrial metabolism in murine CD8+T cells by increasing mitochondrial mass and OXPHOS capacity [27], its global impact on human T cell mitochondrial profiles remains incompletely defined. We therefore analyzed ATP5a, a key ATP synthase subunit required for OXPHOS-dependent ATP generation. Basal ATP5a expression was low across CD8+ T subsets. Metformin markedly elevated ATP5a positivity in CD8+Tcm ($p<0.0001$), Tem ($p<0.001$), Tn($p<0.0001$) and Teff($p<0.01$) cells (Fig.3a-d), indicating universal CD8+T cell ATP5a upregulation. In CD4+T cells, metformin increased ATP5a expression across most subsets, with no significant change detected in Teff cells (Sup Fig. 2a).

To extend our characterization of metformin-driven mitochondrial remodeling beyond OXPHOS protein expression, we quantified mitochondrial mass and membrane potential ($\Delta\Psi m$). MitoTracker Green staining showed that metformin significantly increased mitochondrial mass across all CD8+T subsets ($p<0.01$-0.001; Fig.3e-3f). In CD4+T cells, mitochondrial mass rose in Tn, Teff and Tem populations but remained unchanged in Tcm cells (Sup Fig.2b). TMRE staining further revealed reduced $\Delta\Psi m$ intensity across all CD8+T subsets following metformin treatment ($p<0.05$-0.01; Fig. 3g-3h), with unaltered frequencies of TMRE-positive cells in CD8+Tcm cells. For CD4+T cells, $\Delta\Psi m$ decreased specifically in Tcm and Tn subsets, while Teff and Tem cells were unaffected (Sup Fig. 2c). Together, these findings demonstrate that metformin induces coordinated mitochondrial adaptation in human T cells, concurrently elevating OXPHOS-related protein expression and mitochondrial content while moderately lowering $\Delta\Psi m$ to support metabolic homeostasis.

Metformin differentially regulates mitochondrial and intracellular ROS in T cells

Mitochondrial electron transport chain activity couples ATP synthesis with ROS production. Metformin strengthens anti-tumor vaccine responses in mice by driving FAO-dependent expansion of CD8+memory T cells [28]. Building on our observed metformin-mediated mitochondrial metabolic remodeling, we systematically profiled mitochondrial and total intracellular ROS levels across CD4+ and CD8+T cell subsets. We assessed mtROS abundance via MitoSOX Red staining. Metformin markedly increased the frequency and fluorescence intensity of mtROS-positive cells across all CD8+T subsets, including Tcm, Tem, Tn and Teff cells ($p<0.001$, $p<0.0001$; Fig. 4a-d). Similarly, metformin robustly elevated mtROS levels in all CD4+T cell populations (Sup Fig. 3a-c). These data demonstrate that metformin broadly augments mitochondrial ROS production throughout diverse T cell subsets. We further quantified total intracellular ROS using H2DCFDA staining to determine whether elevated mtROS correlates with global ROS accumulation. Despite enhanced mtROS production, metformin significantly reduced pan-cellular ROS levels in CD8+Tcm cells ($p<0.0001$, Fig.4e), with consistent decreases observed across all other CD8+T subsets (Fig.4f). Metformin also diminished global ROS abundance in CD4+T cells ($p<0.0001$, Sup Fig.3d), revealing divergent regulation of mitochondrial and total cellular ROS by metformin in T cells. These results indicate that metformin differentially remodels T cell redox homeostasis by increasing mitochondrial ROS while reducing global intracellular ROS. Rather than triggering oxidative stress, metformin drives adaptive reprogramming of cellular redox balance.

Metformin markedly upregulates Pentose Phosphate Pathway in Tcm and Tn cell

Elevated ROS depletes cellular NADPH to perturb NADPH/NADP+redox homeostasis, thereby activating G6PD, the rate-limiting enzyme of the pentose phosphate pathway (PPP). G6PD activation redirects G6P flux into the PPP to generate proliferative metabolites and ATP [29], rendering it a core target for metformin-mediated metabolic regulation. We next assessed G6PD expression across CD8+T cell subsets. Basally, CD8+Tcm (38.44%) and Tn (39.68%) cells exhibited high G6PD positivity, while Tem (17.16%) and Teff (16.31%) cells showed markedly lower levels (Fig. 5a). Metformin significantly increased G6PD-positive frequency and MFI across all CD8+T subsets, with Tcm and Tn positivity rising to 65.06% and 65.61%, respectively ($p<0.01$, $p<0.005$, $p<0.0001$; Fig. 5b-5d). Consistent upregulation of G6PD was also detected in CD4+ T cell populations ($p<0.005$, $p<0.0001$; Sup Fig. 4a-4d). G6P partitioning governs the dynamic balance between glycolysis and the PPP. Hexokinase-derived G6P fuels both glycolytic ATP production and PPP-dependent NADPH generation to sustain redox stability and biosynthesis [30]. Metformin-induced ROS elevation and G6PD activation reroute G6P flux toward the PPP. Consistently, intracellular G6P levels were significantly reduced in metformin-treated PBMCs ($p=0.0019$, Fig.5e). These results indicate that metformin lowers cellular G6P abundance while enhancing PPP flux via G6PD activation, predominantly in Tcm and Tn cells.

Metformin enhances the Glut1 and Glut3 expression in T cells

Glut1 is a ubiquitous high-affinity glucose transporter in T cells and other cell types. Flow cytometry of PBMCs from middle-aged donors revealed higher Glut1 expression in CD4+ relative to CD8+T cell subsets (Fig. 6a, 6b, 6d; Sup Fig. 5a-5b). We further assessed metformin-dependent Glut1 regulation across T cell populations. Metformin significantly elevated both the frequency of Glut1-positive cells ($p<0.01$) and Glut1 MFI ($p<0.05$) in CD8+Tcm cells (Fig.6b), whereas CD8+Tn, Teff and Tem cells showed no measurable changes in Glut1 abundance or positivity (Fig.6d). These data indicate that metformin selectively augments Glut1 expression within the CD8+Tcm compartment. Our results revealed subset-dependent Glut1 regulation by metformin. Metformin minimally altered Glut1 expression across all CD4+ T cell subsets (Sup Fig 5b), maintaining stable expression throughout CD4+T cell differentiation. By contrast, metformin selectively promoted Glut1 expression in CD8+Tcm cells but not in CD8+Teff cells. These data indicate that metformin mediates stringent subset-specific Glut1 modulation in human T cells.

Recent work has established that CD8+ T cell proliferation is Glut1-independent, with the high-affinity glucose transporter Glut3 acting as a key determinant of CD8+T cell proliferation and survival [30]. Ectopic Glut3 expression boosts glucose metabolism, energy storage and anti-tumor function in murine CD8+T cells [30,31]. In this study, we systematically profiled Glut3 expression across human T cell subsets and characterized metformin-mediated regulation. Flow cytometry identified predominant Glut3 expression in CD8+Tcm (Fig.6a,6b) and Tn cells (Fig.6a,6d), whereas CD8+Tem and Teff cells exhibited negligible Glut3 positivity (Fig.6a,6c,6e). Glut3 abundance was substantially lower in CD4+T subsets, with only rare Glut3+CD4+Tcm and Tn cells detected (Sup.Fig.5a,5c). Notably, metformin markedly upregulated Glut3 expression across all CD4+ and CD8+T cell populations ($p<0.001$, $p<0.0001$, Fig.6c,6e, Sup Fig.5c). Together, our results reveal distinct subset- and lineage-specific expression patterns of Glut1 and Glut3, with elevated transporter levels in long-lived Tn and Tcm cells, and demonstrate that metformin broadly enhances T cell glucose transporter expression.

Metformin inhibits HK1 Expression in CD8+Tcm and Tn cells

Hexokinase (HK) acts as a rate-limiting glycolytic enzyme that phosphorylates glucose to produce G6P, with HK1 and HK2 serving as the predominant, differentially regulated mammalian isoforms. Metformin enhances OXPHOS by upregulating the ATP synthase subunit ATP5a-particularly in CD8+Tcm and CD8+Tn cells-which elevates the ATP/ADP ratio and consequently suppresses HK1 and HK2 expression. We next investigated metformin-mediated HK1 modulation across T cell subsets. All CD4+ and CD8+ T cell subsets exhibited universal HK1 positivity (Fig. 7a; Sup Fig. 5d), yet metformin induced distinct alterations in HK1 MFI. In CD8+compartments, HK1 MFI was significantly reduced in Tcm (p=0.022, Fig.7b) and Tn cells (p=0.0019, Fig.7d), unaltered in Tem cells (Fig.7c), and increased in Teff cells (p=0.028, Fig.7e). For CD4+T cells, HK1 MFI declined significantly in Tcm (p=0.0137), Tem (p=0.0185) and Tn subsets (p=0.0113), with no changes detected in CD4+Teff cells (Sup Fig. 5e-5h). Due to limited primary PBMC samples, HK2 activity was assessed via ELISA, revealing robust metformin-induced HK2 inhibition (p=0.0003, Fig.7f). Collectively, these results demonstrate that metformin suppresses HK2 activity and exerts subset-specific regulation of HK1 expression across human T cell populations.

Metformin promoted the expression of genes related to FAO metabolism pathway, inhibited the expression of glycolysis associated genes.

We used the R package limma to perform differential gene expression analysis to dissect the molecular basis of metformin-induced cellular phenotypes. With stringent thresholds (adjusted $p < 0.05$, $|\log2FC| > 0.8$), we identified numerous differentially expressed genes (DEGs) between control and metformin-treated groups, with divergent up- and downregulation patterns visualized via volcano plotting (Fig.8a). Heatmap analysis further resolved the DEG expression profiles associated with core metabolic processes. Metformin upregulated *FASN*, *ELOVL5* and *ACSL6*, which mediate long-chain saturated fatty acid synthesis and elongation, supporting glucose-driven lipogenesis in Tcm cells, though the underlying futile metabolic cycle remains incompletely defined [16,17]. Metformin also elevated *ACADM* (critical for mitochondrial β-oxidation) and *ACAT2*, which facilitates cytoplasmic acetoacetyl-CoA production (Fig.8b). Conversely, multiple genes governing fatty acid synthesis and oxidation were repressed, alongside reduced expression of glycolytic regulators *HK1/2/3*, indicating context-dependent metabolic gene regulation by metformin (Fig. 8b). KEGG pathway analysis enriched these DEGs in fatty acid metabolism, amino acid biosynthesis and the pentose phosphate pathway (Fig. 8c). These transcriptomic alterations align with our functional data showing metformin-induced upregulation of the FAO key enzyme CPT1a, linking suppressed glycolytic transcription to enhanced FAO. GO functional enrichment further assigned these DEGs to immune processes, vesicle-mediated transport and enzyme binding (Fig. 8d). Future work is required to elucidate the detailed mechanisms underlying these regulatory events.

Methods and material

Ethics statement

This study was conducted under a waiver of informed consent, approved by the ethics committee. Ethics approval for this study was obtained from the ethics committees of the Zhong Shan Medical School, Sun Yat-San University (Guangzhou, China), and the First Affiliated Hospital of Sun Yat-San University (Guangzhou, China).

Study participants

A total of 215 participants were enrolled at the First Affiliated Hospital of Sun Yat-sen University, Guangzhou, China, and contributed peripheral blood samples to the present study. All participants were aged between 45 and 65 years and were negative for HIV, HBV, and HCV, with no known cancer or active infectious diseases at the time of blood collection.The study involved multiple phenotypic and metabolic assays conducted at various experimental stages. Complete and analyzable T-cell phenotypic data were obtained for 138 participants. Individual metabolic parameters were evaluated in subsets of participants based on sample availability and assay-specific criteria, with the corresponding sample sizes detailed in the figure legends. Among those participants with available HbA1c measurements, the majority exhibited HbA1c levels below 6.5%. All samples were processed under uniform ex vivo experimental conditions to facilitate paired comparisons between untreated and metformin-treated states.

Preparation of PBMCs

PBMCs were isolated by Ficoll-hypaque (Tian Jin Hao Yang Biological Manufacture, China; cat. LTS1077) gradient centrifugation of sodium heparin-blood obtained from HDs. PBMCs were resuspended in complete RPMI 1640 medium (GIBCO, cat.C11875500BT) supplemented with 10% Fetal Bovine Serum (Biological Industries, cat.04–011-1ACS), 1% Penicillin–Streptomycin (GIBCO, cat.15140–122).

Flow cytometry

Phenotypic characterization: PBMCs cultured with 20 mmol metformin (GLPBIO, cat. GC60245) at 37°C for 24 h were stained for phenotypic analyses. The following panel of mouse anti-human mAbs was used: APC.cy7-conjugated anti-CD3 (TONBO biosciences, 25–0038-T100), Percp.cy5.5-conjugated anti-CD8 (TONBO biosciences, 65–0088-7100), Alexa Fluor 700-conjugated anti-CD45RA (BD Pharmingen, 560673), Brilliant Violet 510-conjugated anti-CCR7 (Biolegend, 353232). All samples were collected on FACS Aria II BD (Mountain View, CA, USA). Data were analyzed using Flow Jo software (Tree Star, San Carlos, CA, USA).

Flow Cytometric Sorting: We treated isolated PBMCs with 20 mM metformin or untreated. The samples were incubated for 30 minutes at 4°C in the dark with the following antibodies: APC.cy7-conjugated anti-CD3 (TONBO biosciences, 25–0038-T100), Percp.cy5.5-conjugated anti-CD8 (TONBO biosciences, 65–0088-7100), and Brilliant Violet 510-conjugated anti-CCR7 (Biolegend, 353232). CD3+CD8+CCR7+ cell populations were sorted using a flow cytometer.

Metabolic Assays

G6P Detection Assay (WST-8): A G6P assay kit (Beyotime, S0185) was utilized to measure glucose-6-phosphate (G6P) levels in the medium of PBMCs with metformin treatment or control. The assay involves the conversion of G6P to 6-phosphogluconate by glucose-6-phosphate dehydrogenase, coupled with the reduction of WST-8 to a formazan dye, which is measurable at 450 nm. The assay procedures were performed according to the manufacturer's instructions.

Hexokinase 2 (HK2) Enzyme-Linked Immunosorbent Assay: A Hexokinase 2 (HK2) ELISA kit (Cloud-Clone, SED352Hu) was utilized to quantify hexokinase 2 (HK2) levels in the medium of

CD3+CD8+CCR7+ PBMCs with metformin treatment or control. The assay employs a double-antibody sandwich method to ensure specificity and sensitivity. The assay procedures were performed according to the manufacturer's instructions.

Flow-based metabolic assays

Due to spectral limitations associated with AF488-conjugated antibodies, each metabolic marker was assessed in a separate batch of donor samples. The total number of unique donors across all experiments was 140. Specifically, the number of donors per assay was as follows: ATP5a (n = 20), CPT1a (n = 23), G6PD (n = 17), Glut1 (n = 21), Glut3 (n = 19), HK1 (n = 20), and ROS (n = 20). (see Table)

Met-Flow: Six metabolic proteins were chosen and optimized based on their critical role in specific metabolic pathways. 2×10^6 Cells were harvested and intracellularly stained according to the protocol of eBioscience Intracellular Fixation & Permeabilization Buffer Set (eBioscience, cat.88–8824-00). The following panel of mouse anti-human mAbs was used: Alexa Fluor 488-conjugated anti-G6PD (Santa Cruz, sc-373886), Alexa Fluor 488-conjugated anti-Hexokinase 1(Abcam, ab184818), Alexa Fluor 488-conjugated anti-Glut3, CoraLite Plus 488-conjugated ATP5A1 (Proteintech, CL488-66037), CoraLite Plus 488-conjugated Glut1(CL488-66290), CoraLite Plus 488-conjugated CPT1A(CL488-66039). All samples were collected on FACSAria II BD (Mountain View, CA, USA). Data were analyzed using Flow Jo software (Tree Star, San Carlos, CA, USA).

ROS assays: After 20mM metformin (GLPBIO, GC60245-10) treatment, PBMCs were incubated at 2×10^6 cells per well in RP10 media (RPMI, 10% Foetal Bovine Serum, 1% Penicillin–Streptomycin) alone for 4–6 h at 37°C.Mitochondrial ROS production was measured with MitoSOX RED (Thermo Fisher, M36007) according to the manufacturer's instructions. 2×10^6 cells were incubated in staining buffer (Pansa, TNB-4222-L500) and 500nM MitoSOX RED for 30 minutes at 4°C. After incubation, cells were washed twice in a flow cytometry buffer, and the surface was stained with antibodies for 20 minutes on ice. Fluorescence was acquired immediately after surface staining was performed. All samples were collected on FACSAria II BD (Mountain View, CA, USA). Data were analyzed using Flow Jo software (Tree Star, San Carlos, CA, USA).

Mitochondrial activity assessment: After treatment with 20 mM metformin for 1 day, approximately 1×106 PBMCs were harvested for assessment of mitochondrial mass and mitochondrial membrane potential. For mitochondrial mass assessment, cells were stained with MitoTracker™ Green FM (Thermo Fisher Scientific, cat.M46750) according to the manufacturer's instructions. Briefly, the dye was reconstituted in 20 μL DMSO, and 1 μL of the reconstituted dye was added to cells suspended in 1 mL PBS. For mitochondrial membrane potential assessment, cells were stained with 100 nM tetramethylrhodamine ethyl ester perchlorate (TMRE; MedChemExpress, cat.HY-D0985A). Cells were incubated with the corresponding mitochondrial dye at 37°C for 30 min in the dark, followed by surface antibody staining. After staining, cells

were resuspended in 400 μL PBS for flow cytometric analysis. Samples were acquired on an Attune NxT Flow Cytometer, and data were analyzed using FlowJo software (Tree Star, San Carlos, CA, USA).

RNA seq

Sequencing of mRNA: Middle-age samples (n=3) were ground under liquid nitrogen in a mortar and pestle, and the resulting powder dissolved in TRIzol™ Reagent (Invitrogen, Carlsbad, CA, USA), then extracted total RNA. The quality and purity of RNA were examined by a NanoDrop™ One/OneC spectrophotometer (Thermo Scientific, Waltham, MA, USA) and Life Invitrogen Qubit RNA BR (Broad-Range) Assay Kit. RNA integrity was analyzed using the Agilent 4200 TapeStation system (Agilent, Santa Clara, CA, USA). The NEBNext® Poly(A) mRNA Magnetic Isolation Module and NEBNext® Ultra™ II mRNA Library Prep Kit for Illumina® were used for mRNA isolation and library construction following the manufacturer's protocols. High-throughput transcriptome sequencing was performed on an Illumina NovaSeq 6000 platform according to the manufacturer's instructions.

Identification of differentially expressed genes: The TPM (Transcripts Per Million) data from mRNA sequencing were normalized. Using the "limma" R package, we identified differentially expressed genes between the control and metformin treatment groups. The selection criteria were set with a threshold of $|\log2(\text{fold change})| > 0.8$ and an adjusted p-value < 0.05.

Functional enrichment analysis of DEGs: For functional enrichment analysis of differentially expressed genes (DEGs), we employed the "org.Hs.eg.db" R package for GO annotation. The most up-to-date gene annotations for KEGG pathways were retrieved using the KEGG REST API (https://www.kegg.jp/kegg/rest/keggapi.html) to establish the background dataset. Genes were then mapped to this background, and enrichment analysis was carried out using the "clusterProfiler" R package to derive GO and KEGG enrichment results.

Discussion

Age-related T-cell dyshomeostasis, including shifts in naïve/memory balance and metabolic regulation, progresses across adulthood. We observed that CD8+Tcm decline in middle-aged individuals, whereas CD4+Tcm increase with age [4]; metformin exerts anti-senescence effects and promotes proliferation of undifferentiated T cells [4]. As a first-line antidiabetic agent, metformin also promotes memory T-cell differentiation in mice and correlates with increased tumor-infiltrating lymphocytes, yet the mechanisms governing its regulation of human T-cell metabolism remain unclear.

In this study, our findings demonstrated that metformin selectively expanded CD8+Tcm in PBMCs from middle-aged individuals without affecting CD8+Tem or CD4+memory cells, mirroring subset-specific metabolism: Tcm rely on FAO/OXPHOS, whereas Tem depend on glycolysis [7]. Notably, CPT1a was highly expressed across naïve, memory, and effector subsets; metformin enhanced its MFI in all CD8+subsets yet significantly increased CD4+Tcm and Tn cells. This disparity may reflect lower basal CPT1a expression in CD8+cells, though the underlying

regulatory mechanisms require further investigation.

Our findings revealed that human T cell subsets exhibit distinct metabolic profiles, with higher ATP5a levels in CD4+ than CD8+T cells in PBMC, reflecting lineage-intrinsic bioenergetic tuning. Metformin preferentially elevated ATP5a in CD8+Tcm and naive T cells over CD8+Tem cells, enforcing subset-biased metabolic reprogramming. Combined CPT1a and ATP5a analyses revealed lineage-dependent metformin responsiveness: CD8+T cells showed broad upregulation of both markers, while CD4+T cells exhibited modest CPT1a changes but universal ATP5a induction, suggesting preferential targeting of mitochondrial biogenesis over FAO machinery in CD8+T cells. Metformin also increased mitochondrial content alongside ATP5a elevation. In long-lived memory T cells, an enlarged mitochondrial pool typically correlates with enhanced metabolic reserve and rapid energy mobilization upon restimulation, an adaptive feature supporting longevity [32]; however, increased mass may alternatively reflect impaired mitochondrial turnover and compensatory accumulation of damaged organelles [33]. Here, the increased mitochondrial content coincided with elevated CPT1a, ATP5a, and enhanced redox activity, indicating comprehensive metabolic remodeling rather than inactive accumulation, consistent with an adaptive mitochondrial response. Nevertheless, MitoTracker Green alone cannot distinguish biogenesis from decreased turnover; direct assessment of PGC-1α, TFAM, or mtDNA content, together with mitophagy and turnover measurements, is required to determine whether the expanded mass reflects physiological expansion or compensatory accumulation.

Metformin-driven mitochondrial expansion in CD8+T cells was coupled with mild reductions in mitochondrial membrane potential (ΔΨm) (TMRE). As ΔΨm arises from dynamic electron transport chain proton flux rather than serving as a linear readout of mitochondrial abundance or function, moderate depolarization does not equate to organelle dysfunction [34]. The discordance between increased mitochondrial mass and reduced TMRE signal uncouples mitochondrial quantity from membrane energetic status, demonstrating that metformin induces qualitative functional remodeling rather than uniform mitochondrial activation. Together with elevated CPT1a and ATP5a expression, this profile reflects adaptive metabolic reprogramming. Given progressive mitochondrial dysregulation during immune aging, this retained T cell metabolic plasticity in middle-aged individuals highlights a pre-senescent immune-metabolic regulatory mechanism [35,36]. Further functional profiling, including oxygen consumption, ATP-linked respiration, spare respiratory capacity and mitochondrial quality surveillance, is essential to discriminate adaptive remodeling from compensatory mitochondrial dysfunction. While cellular ROS derive from multiple sources [37], murine studies establish mtROS as a critical mediator of metformin-induced CD8+memory T cell differentiation, acting via Glut1 and Nrf2 activation to support fatty acid oxidation-dependent memory programming [12,24]. Our data show metformin-elicited mtROS elevation coincides with increased mitochondrial mass and ATP5a expression across CD8+T cell subsets, demonstrating that mtROS induction is integral to adaptive mitochondrial reprogramming rather than non-specific oxidative stress.

Metformin treatment elevated mitochondrial ROS (mtROS) but reduced global intracellular ROS in CD8+T cells, reflecting compartment-specific redox regulation rather than conflicting redox states. Mitochondrial ROS act as pro-adaptive metabolic signals, whereas excessive cytoplasmic ROS drives oxidative damage and T cell dysfunction. This divergent redox profile prompted investigation of antioxidant pathway engagement. The pentose phosphate pathway (PPP), via its rate-limiting enzyme G6PD, generates NADPH to sustain major cellular antioxidant systems and maintain redox homeostasis. Metformin upregulated G6PD across CD8+T cell subsets, including Tcm cells. The concomitant G6PD induction, enhanced PPP activity and reduced intracellular ROS indicates that metformin-elicited mitochondrial remodeling is coupled to amplified antioxidant capacity. This coordinated mtROS-dependent metabolic reprogramming and PPP-mediated redox buffering preserves T cell metabolic flexibility in middle age, supporting sustained cellular function and redox balance during immune aging.

We further examined metformin-mediated glycolysis-to-PPP metabolic rewiring in human CD8+Tcm cells. Previous studies in cancer cells have shown that metformin can directly inhibit HK2 activity, potentially through a G6P-mimetic mechanism [38,39], we assessed HK expression in middle-aged PBMCs. Consistent with prior reports, metformin reduced bulk HK2 expression, though subset-specific HK2 profiling was limited by cell availability and warrants future validation. Distinct from HK2, HK1 exhibits subset-restricted distribution and facilitates mitochondrial metabolite uptake in CD8+T cells [40,41]. We found ubiquitous HK1 expression in circulating T cells, while metformin selectively diminished the MFI of HK1 in quiescent Tcm, naive and CD4+ Tem populations. In contrast, HK1 levels remained unaltered in activated Teff cells. These data indicate that metformin suppresses glycolysis primarily within long-lived, quiescent T cell subsets without perturbing glycolytic metabolism in effector T cells.

Accumulating evidence indicates that cytoplasmic dissociation of HK1 redirects G6P flux toward the pentose phosphate pathway (PPP) [42], G6PD acts as a rate-limiting enzyme in the oxidation phase of the PPP. In metformin-treated human PBMCs, CD8+Tcm and naive T cells exhibited elevated G6PD and reduced HK1 expression, supporting a metabolic shift from glycolysis to oxidative PPP. By contrast, CD8+Teff cells displayed concurrent upregulation of both G6PD and HK1 upon metformin exposure (Figure 7). The oxidative PPP consumes G6P to produce NADPH, whereas the non-oxidative PPP generates glycolytic intermediates [43]. Metformin reduced global G6P abundance in PBMCs, consistent with enhanced G6P consumption via oxidative PPP in quiescent CD8+T subsets. One explanation was the CD8+Tcm and CD8+Tn cells in favor of oxidizing the PPP pathway, and G6P was consumed as the substrate of PPP. In the CD8+Teff cells, we speculated that G6P was converted to glycolytic intermediates through the PPP non-oxidizing pathway, and further work is needed to determine the fructose-6-phosphate and aldehyde-3-phosphate expression.

Despite emerging knowledge of T cell metabolism, a systematic metabolic landscape across human T cell subsets remains poorly defined. Here, we profile the comprehensive metabolic spectrum of human T cells. We show that metformin-driven CD8+Tcm expansion relies on coordinated metabolic reprogramming encompassing mitochondrial oxidative metabolism, redox homeostasis and pentose phosphate pathway-linked glucose metabolism. Importantly, these

adaptive metabolic changes are retained in T cells from middle-aged individuals, indicating sustained metabolic plasticity during the onset of age-associated immune deterioration. Our findings suggest that exogenous interventions exemplified by metformin-mediated metabolic modulation can counter immune ageing in middle age, thereby boosting immune responses in vaccination, chronic viral infection and cancer immunotherapy.

Reference

1. Lam N, Lee Y, Farber DL. A guide to adaptive immune memory. Nat Rev Immunol. 2024;24(11):810-829.
2. Vandana K, Surojit S,Tania SG, et al. Differentiation of memory B and T cells. Curr Opin Immunol. 2006;18(3):255–264.
3. Kumar BV, Connors TJ, Farber DL. Human T Cell Development, localization, and function throughout Life. Immunity. 2018; 48:202–13.
4. Yang J, Liu HC, Zhang JQ, et al. The effect of metformin on senescence of T lymphocytes. Immun Ageing. 2023;20(1):73.
5. Farber DL, Yudanin NA, Restifo NP. Human memory T cells: generation, compartmentalization and homeostasis. Nat Rev Immunol. 2014;14(1):24-35.
6. Smith SH, Brown MH, Rowe D, et.al. Functional subsets of human helper-inducer cells defined by a new monoclonal antibody, UCHL1. Immunology.1986;58:63–70.
7. O'NeillL A, Kishton RJ, Rathmell J. A guide to immunometabolism for immunologists. Nat Rev Immunol. 2016:16:553-565.
8. Chapman NM, Boothby MR, Chi H. Metabolic coordination of T cell quiescence and activation. Nat Rev Immunol. 2020;20(1):55-70.
9. Van der WGJ , Bart E, Chih-Hao Ch, et al. Mitochondrial respiratory capacity is a critical regulator of CD8+ T cell memory development. Immunity.2012; 36: 68–78.
10. O'Sullivan D, van der WGJ, Huang SC, et al. Memory CD8+ T cells use cell intrinsic lipolysis to support the metabolic programming necessary for development. Immunity.2014; 41:75–88.
11. Guoliang C , Matthew M S , Simon M G , et al. IL-7-induced glycerol transport and TAG synthesis promotes memory CD8+ T cell longevity. Cell. 2015;161: 750–761.
12. Pearce EL, Walsh MC, Cejas PJ, et al. Enhancing CD8 T- cell memory by modulating fatty acid metabolism. Nature.2009; 460:103–107.
13. Glenn R B , Lorenzo G, Guido K,et al. The spectrum of T cell metabolism in health and disease. Nat Rev Immunol. 2018; 18(1):19-34.
14. Anthony TP, Andrew LD, Asis P, et al. Constitutive glycolytic metabolism supports CD8+ T cell effector memory differentiation during viral infection. Immunity.2016; 45: 1024–1037.
15. Patricia G , Veit RB , Christian S, et al. Serial transfer of single-cell-derived immunocompetence reveals stemness of CD8+ central memory T cells. Immunity.2014; 41:116–126.
16. Corrado M, Pearce EL. Targeting memory T cell metabolism to improve immunity. J Clin Invest. 2022;132(1): e148546.
17. Christopher E , Lili G , Stefana V , et al . Differential reliance on lipid metabolism as a salvage pathway underlies functional differences of T cell subsets in poor nutrient environments. Cell Rep. 2018;23(3):741–755.
18. Maija T , Sofia R, Kai K.et al. Metformin Alleviates Inflammation and Induces Mitophagy in

Human Retinal Pigment Epithelium Cells Suffering from Mitochondrial Damage. Cells. 2024;13(17):1433.
19. Triggle, CR, Mohammed, I, Bshesh, K, et al. Metformin: Is It a Drug for All Reasons and Diseases? Metabolism. 2022;133: 155223.
20. Nojima I, Wada J. Metformin and Its Immune-Mediated Effects in Various Diseases, Int J Mol Sci. 2023;24(1):755.
21. Ameya S K , Sriram G , Nir B. Benefits of Metformin in Attenuating the Hallmarks of Aging, Cell Metab. 2020;32(1):15-30.
22. Nojima I, Wada J. Metformin and Its Immune-Mediated Effects in Various Diseases, Int J Mol Sci. 2023;24(1):755.
23. Araki K, Turner AP, Shaffer VO, et al. mTOR regulates memory CD8 T-cell differentiation. Nature.2009; 460: 108-112.
24. Mikako N , Nahoko Y, Taisaku O,et al. Mitochondrial reactive oxygen species trigger metformin-dependent antitumor immunity via activation of Nrf2/mTORC1/p62 axis in tumor-infiltrating CD8T lymphocytes. J Immunother Cancer. 2021;9(9): e002954.doi: 10.1136/jitc-2021-002954.
25. Nojima I, Wada J. Metformin and Its Immune-Mediated Effects in Various Diseases. Int J Mol Sci. 2023;24(1):755.
26. Pearce EL, Pearce EJ. Metabolic pathways in immune cell activation and quiescence. Immunity. 2013;38(4):633-43.
27. Böhme J, Martinez N, Li S, et al. Metformin enhances anti-mycobacterial responses by educating CD8+ T-cell immunometabolic circuits. Nat Commun. 2020;11(1):5225.
28. Julio FT. Mitochondrial formation of reactive oxygen species. J Physiol. 2003;552(Pt 2):335-44.
29. Wei Hai Y.NAD+/NADH and NADP+/NADPH in cellular functions and cell death: regulation and biological consequences. Antioxidants & Redox Signaling. 2008(10) 2, DOI: 10.1089/ars.2007.1672
30. Sicong M, Yanan M, Jingxia W, et al. Cellular metabolism regulates the differentiation and function of T-cell subsets. Cellular & Molecular Immunology.2024;21:419–435
31. Elisabetta C, Greta MPGA, Pierpaolo G, et al. Enforcing GLUT3 expression in CD8+ T cells improves fitness and tumor control by promoting glucose uptake and energy storage.Frontiers in Immunology, 2022.
32. Wu Z, Yu M, Leary SC, Yuan J, Huang J, Xiang J. TGF-β Regulates CD8+ T Cell Memory by Triggering mTORC1Weak-Mediated Activation of the Transcriptional FOXO1-TCF1-Eomes and Metabolic AMPK-ULK1-ATG7 Pathways. Cells. 2026;15(5):471.
33. Zhang R, Gao F, Li J, et al. USP30 inhibition augments mitophagy to prevent T cell exhaustion. Sci Adv. 2025;11(33):eadv6902.
34. Kowaltowski AJ, Abdulkader F. How and when to measure mitochondrial inner membrane potentials. Biophys J. 2024 Dec 17;123(24):4150-4157. doi: 10.1016/j.bpj.2024.03.011. Epub 2024 Mar 7.
35. Luo L, Lechuga-Vieco AV, Sattentau C, Borsa M, Simon AK. Dysfunctional mitochondria in ageing T cells: a perspective on mitochondrial quality control mechanisms. EMBO Rep. 2025;26(18):4402-4418.

36. Denk D, Singh A, Kasler HG, et al. Effect of the mitophagy inducer urolithin A on age-related immune decline: a randomized, placebo-controlled trial. Nat Aging. 2025;5(11):2309-2322.
37. Cheung EC, Vousden KH. The role of ROS in tumour development and progression. Nat Rev Cancer. 2022;22(5):280-297.
38. Scott J , James NW, Bernard R. Subcellular localization of hexokinases I and II directs the metabolic fate of glucose, PLoS One.2011; 6:(3) e17674.
39. Salani B, Marini C, Rio AD, et al. Metformin impairs glucose consumption and survival in Calu-1 cells by direct inhibition of hexokinase-II. Sci Rep. 2013;3:2070.
40. Valerie AG, Rigel JK, Amanda GN. Metabolic programming and PDHK1 control CD4+T cell subsets and inflammation. J Clin Invest. 2015;125(1):194–207.
41. Glenn RB , Marco F Jasmin G. Mitochondria–ER contact sites are immunometabolic hubs that orchestrate the rapid recall response of memory CD8+ T cells. Immunity.2018; 48: 542–555.
42. De JA, Keyhani NF, Pusec MC, et al. Hexokinase 1 cellular localization regulates the metabolic fate of glucose. Mol Cell. 2022; 82(7): 1261–1277.
43. TeSlaa T, Ralser M, Fan J, et al. The pentose phosphate pathway in health and disease, Nat Metab. 2023; 5(8): 1275–1289.

Figure Legends

Figure 1 Metformin remodels human CD4+ and CD8+ T cell subset distribution. (a) Representative flow cytometry plots depicting Tn, Tcm, Tem and Teff profiles within human CD3+CD4+ and CD3+CD8+T cells under control and metformin-treated conditions. (b,c) Frequency (b) and absolute counts with relative control ratios (c) of CD8+Tcm cells in the presence or absence of metformin. (d, e) Frequencies of CD8+ (d) and CD4+ (e) T cell subsets following metformin treatment. Data are mean ± SEM; statistical analyses were performed using paired tests. **$p < 0.01$, ****$p < 0.0001$. Tn, naive T cell; Tcm, central memory T cell; Tem, effector memory T cell; Teff, effector T cell; Met, metformin.

Figure 2 Metformin upregulates CPT1a expression in human CD8+ T cell subsets. Representative flow cytometry analyses and frequencies of CPT1a+cells in CD8+Tcm (a), Tem (c), Tn and Teff (e) subsets under control and metformin treatment. CPT1a MFI was quantified in CD8+ Tcm (b), Tem (d), Tn and Teff (f) cells. Data are mean ± SEM; paired t-test, *$p < 0.05$, **$p < 0.01$, ***$p < 0.005$. Tn, naive T cell; Tcm, central memory T cell; Tem, effector memory T cell; Teff, effector T cell.

Figure 3 Metformin reshapes mitochondrial metabolic features in human CD8+ T cell subsets. (a–d) Representative flow cytometry plots and quantified frequencies of ATP5a+CD8+Tcm, Tem, Tn and Teff cells under control and metformin-treated conditions. (e, f) Representative plots and quantification of MitoTracker Green (MTG) geometric MFI (gMFI) in CD8+Tcm, Tn, Teff and Tem subsets. (g,h) Representative plots and fold-change gMFI of TMRE staining in CD8+Tcm, Tn, Teff and Tem cells. Data are mean ± SEM; paired t-test, *$p < 0.05$, **$p < 0.01$, ***$p < 0.001$, ****$p < 0.0001$. MTG, MitoTracker Green; TMRE, tetramethylrhodamine ethyl ester perchlorate;

gMFI, geometric mean fluorescence intensity.

Figure 4 Metformin differentially modulates mitochondrial and global ROS levels in human CD8+ T cell subsets. (a–d) Representative flow cytometry plots, positive frequencies and gMFI of mtROS in control and metformin-treated CD8+Tcm, Tem, Tn and Teff cells. (e,f) Representative histograms and quantitative analysis of H2DCFDA-based global ROS gMFI across CD8+ T subsets. Data are mean ± SEM; paired t-test, *p < 0.05, ***p < 0.001, ****p < 0.0001. mtROS, mitochondrial reactive oxygen species; gMFI, geometric mean fluorescence intensity; Met, metformin.

Figure 5 Metformin upregulates G6PD expression in human CD8+ T cell subsets. (a) Representative flow cytometry analysis of identifying G6PD-positive cells within CD8+ T subsets under control and metformin-treated conditions. (b-d) Quantification of G6PD-positive frequencies and MFI across CD8+T cell subsets. (e) Relative changes in extracellular G6P levels in metformin-treated human PBMCs. Data are mean ± SEM; paired t-test, **p < 0.01, ***p < 0.001, ****p < 0.0001. Tn, naive T cell; Tcm, central memory T cell; Tem, effector memory T cell; Teff, effector T cell.

Figure 6 Metformin modulates Glut1 and Glut3 expression in human CD8+ T cell subsets. (a) Representative flow cytometry histograms of Glut1 and Glut3 expression in CD8+Tcm, Tn, Tem and Teff cells under control and metformin treatment. (b, c) Quantification and relative fold changes of Glut1 (b) and Glut3 (c) positivity and MFI in CD8+Tcm cells. (d, e) Frequencies and gMFI of Glut1 (d) and Glut3 (e) across CD8+ Tn, Tem and Teff subsets. Data are mean ± SEM; paired t-test, *p < 0.05, **p < 0.01, ***p < 0.001, ****p < 0.0001.

Figure 7 Metformin mediates subset-specific HK1 regulation in CD8+T cells and suppresses HK2 abundance in human PBMCs. (a) Representative flow cytometry histograms of HK1 expression across CD8+Tcm, Tem, Tn and Teff subsets under control and metformin treatment. (b-e) Quantified gMFI of HK1 in individual CD8+T cell subsets following metformin exposure. (f) ELISA-based quantification of HK2 levels in control and metformin-treated PBMC lysates. Data are mean ± SEM; paired t-test, *p < 0.05, **p < 0.01, ***p < 0.001.

Figure 8 Identifying Differential Genes and Functional Enrichment between the Control Group and the Met-Treated Group.
(a) Volcano plot illustrating differentially expressed genes (DEGs): red indicates upregulated genes, blue signifies downregulated genes, and gray denotes genes with non-significant changes. (b) Heatmap depicting genes associated with fatty acid metabolism and the pentose phosphate pathway. (c, d) Functional enrichment analysis of DEGs was conducted using KEGG (c) and GO (d) analyses.

Supplementary Figure 1 Metformin selectively modulates CPT1a expression in human CD4+T cell subsets. (a) Flow cytometry gating strategy for CD4+ and CD8+ T cell subsets, with FMO and unstained controls applied for standardized CCR7 gating. (b-d) Representative plots, frequencies and fold-change MFI of CPT1a in control and metformin-treated CD4+Tcm and Tem cells. (e) Representative flow cytometry plots and quantitative analysis of CPT1a expression in CD4+Tn

and Teff subsets. Data are mean ± SEM; paired t-test, *p < 0.05. FMO, fluorescence minus one; MFI, mean fluorescence intensity; Tn, naive T cell; Tcm, central memory T cell; Tem, effector memory T cell; Teff, effector T cell.

Supplementary Figure 2 Metformin remodels mitochondrial properties in human CD4+ T cell subsets. (a) Representative histograms and frequency quantification of ATP5a expression across CD4+T cell subsets under control and metformin treatment. (b, c) Flow cytometric quantification of MTG (b) and TMRE (c) gMFI in CD4+ T cells with or without metformin exposure. Data are mean ± SEM; paired t-test, *p < 0.05, **p < 0.01, ***p < 0.001, ****p < 0.0001.

Supplementary Figure 3 Metformin differentially regulates mitochondrial and global ROS levels in human CD4+ T cell subsets. (a-c) Representative flow cytometry plots, positive frequencies and fold-change gMFI of mtROS in control and metformin-treated CD4+Tcm, Tem, Tn and Teff cells. (d) Representative histograms and quantitative analysis of H2DCFDA-based global ROS MFI across CD4+ T cell subsets. Data are mean ± SEM; paired t-test, ***p < 0.001, ****p < 0.0001. mtROS, mitochondrial reactive oxygen species; gMFI, geometric mean fluorescence intensity; MFI, mean fluorescence intensity; Met, metformin.

Supplementary Figure 4 Metformin increases G6PD expression in human CD4+ T cell subsets. (a) Flow cytometry gating strategy to identify G6PD-positive populations within CD4+ T cell subsets under control and metformin-treated conditions. (b–d) Quantification of G6PD-positive frequencies and MFI across distinct CD4+ T cell subsets. Data are mean ± SEM; paired t-test, ***p < 0.001, ****p < 0.0001. Tn, naive T cell; Tcm, central memory T cell; Tem, effector memory T cell; Teff, effector T cell.

Supplementary Figure 5 Metformin induces distinct subset-specific changes in Glut1, Glut3 and HK1 expression across human CD4+ T cell populations. (a) Representative contour plots showing Glut1 and Glut3 expression in CD4+ T cell subsets under control and metformin treatment. (b,c) Quantification of Glut1 (b) and Glut3 (c) positive frequencies and MFI across CD4+ T cell subsets. (d–h) Representative plots and quantified MFI of HK1 expression in CD4+ Tcm, Tem, Tn and Teff subsets with or without metformin exposure. Data are mean ± SEM; paired t-test, *p < 0.05, **p < 0.01, ***p < 0.001, ****p < 0.0001.

Acknowledgements:

We gratefully thank all the patients and their families who participated in this study. We thank other members of the laboratory for their assistant. Graphical abstract was generated using BioRender.

Authors' contributions:

X.F.H. involving in conceiving the project, performed experiments, including FAO, OXPHOS, Glycolysis related enzyme detection; H.C.L. performed experiments involving isolation of PBMCs, the phenotype detection, ROS detection and data analysis; S.Z.Q. collected peripheral blood of Healthy Donors, analysis of RNA-seq data analysis and contributed to manuscript preparation. J.Q.Z., S.J.C., C.G.L, prepared and collected clinical samples and data analysis; J.X.T., H.R.Y.,

Participated in chart preparation/creation; Y.G. designed experimental and prepared the manuscript; H.H. conceived, designed, and supervised experimental procedures and prepared the manuscript. All authors reviewed the manuscript.

Funding

This study was supported by: National Natural Science Foundation of China 32170810, National Natural Science Foundation of China 82373783.

Availability of data and materials

All data generated or analyzed during this study are included in this published article.

Declarations

The experimental protocol was established, according to the ethical guidelines of the Helsinki Declaration and was approved by the Human Ethics Committee of Sun Yat-sen University. Written informed consent was obtained from individual or guardian participants.

Consent for publication

Not applicable.

Competing interests

The authors declare no competing interests.

Table1. Demographic and clinical characteristics of participants included in the phenotypic analysis

Characteristic	Phenotypic cohort (n = 138)
Age, years	53.59 ± 5.80
Age range, years	45–65
Male, n (%)	66 (47.8%)
Female, n (%)	72 (52.2%)
HbA1c available, n (%)	125 (90.6%)
HbA1c, %	5.72 ± 0.66
HbA1c <6.5%, n (%)	117 (93.6%)
HbA1c ≥6.5%, n (%)	8 (6.4%)

HbA1c measurements were available for 125 of the 138 participants included in the phenotypic analysis, with a mean HbA1c level of 5.72 ± 0.66%. The majority of participants with available HbA1c measurements had HbA1c levels below 6.5% (117/125, 93.6%) .

Table 2. Demographic characteristics and sample distribution across individual experimental analyses

	Experimental analysis	Sample, n（%）	mean ± SD	Age range, years	P value
Age, years	GLUT1	20 (10.6%)	53.95 ± 6.39	45–63	0.063
	ATP5A	19 (10.1%)	54.68 ± 5.35	45–64	
	CPT1A	23 (12.2%)	53.83 ± 6.14	45–65	
	MitoSOX Red (mtROS)	20 (10.6%)	54.05 ± 6.38	45–63	
	HK1	20 (10.6%)	52.90 ± 5.30	47–65	
	GLUT3	19 (10.1%)	55.16 ± 6.28	45–65	
	G6PD	17 (9.0%)	50.24 ± 3.25	45–56	
	MitoTracker Green	13 (6.9%)	53.31 ± 3.01	49–61	
	TMRE	10 (5.3%)	56.50 ± 6.15	47–64	
	H2DCFDA	10 (5.3%)	51.70 ± 3.83	46–57	
	G6P	12 (6.3%)	53.83 ± 5.04	48–64	
	HK2	6 (3.2%)	59.33 ± 5.99	50–65	
Sex	Male	91（48.1%）	—	—	0.959
	Female	98（51.9%%）	—	—	
Overall experimental samples	—	189	53.83 ± 5.62	45–65	—

Data are presented as mean ± SD, range, or n (%), as appropriate. Age was compared across the 12 experimental cohorts using one-way analysis of variance (ANOVA), and sex distribution was compared using the chi-square test. No significant differences were observed in age (P = 0.063) or sex distribution (P = 0.959) among the experimental cohorts. The overall experimental sample size (n = 189) represents the sum of samples used across the individual experimental analyses. mtROS, mitochondrial reactive oxygen species; HK, hexokinase; G6PD, glucose-6-phosphate dehydrogenase; G6P, glucose-6-phosphate.

Figure 1

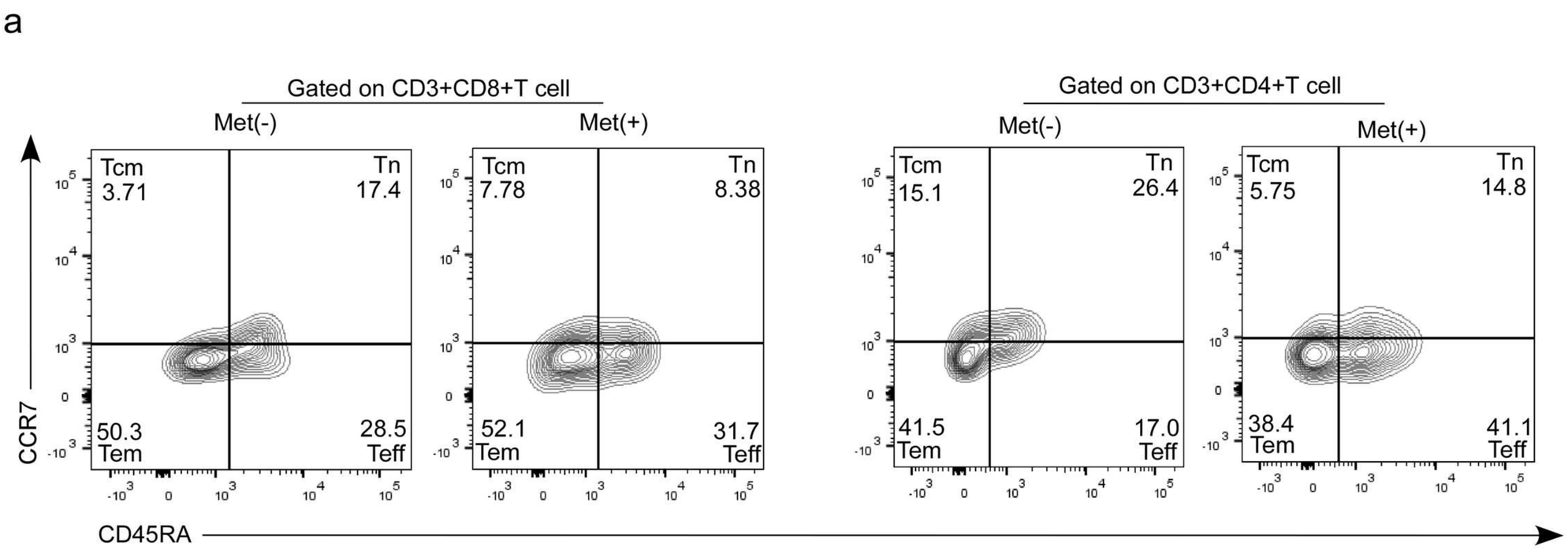
a
Gated on CD3+CD8+T cell
Met(-)
Met(+)
Gated on CD3+CD4+T cell
Met(-)
Met(+)
Tcm 3.71
Tn 17.4
50.3 Tem
28.5 Teff
Tcm 7.78
Tn 8.38
52.1 Tem
31.7 Teff
Tcm 15.1
Tn 26.4
41.5 Tem
17.0 Teff
Tcm 5.75
Tn 14.8
38.4 Tem
41.1 Teff
CCR7
CD45RA

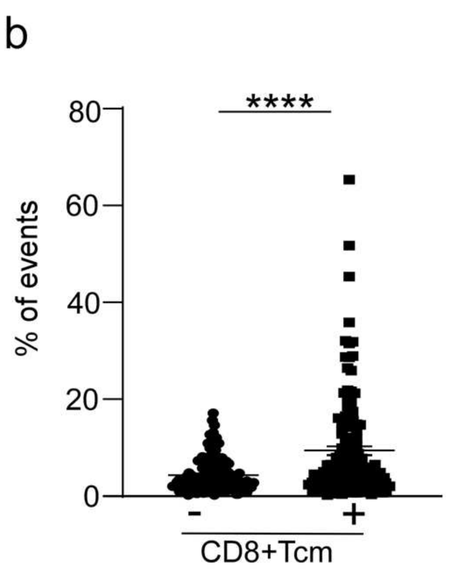
b
****
% of events
CD8+Tcm

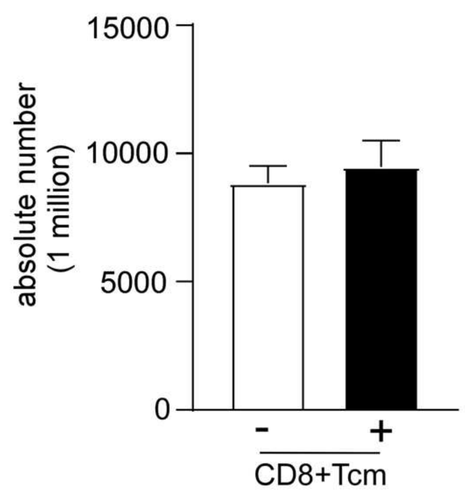
c
absolute number (1 million)
CD8+Tcm

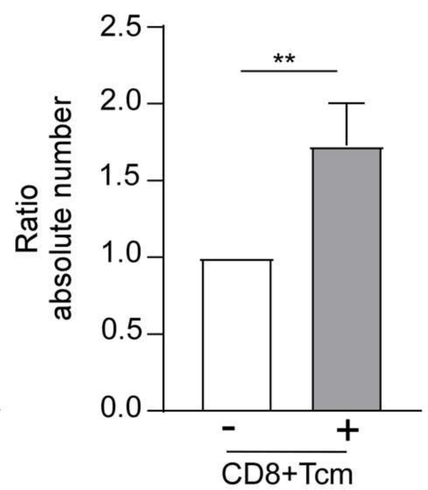
**
Ratio absolute number
CD8+Tcm

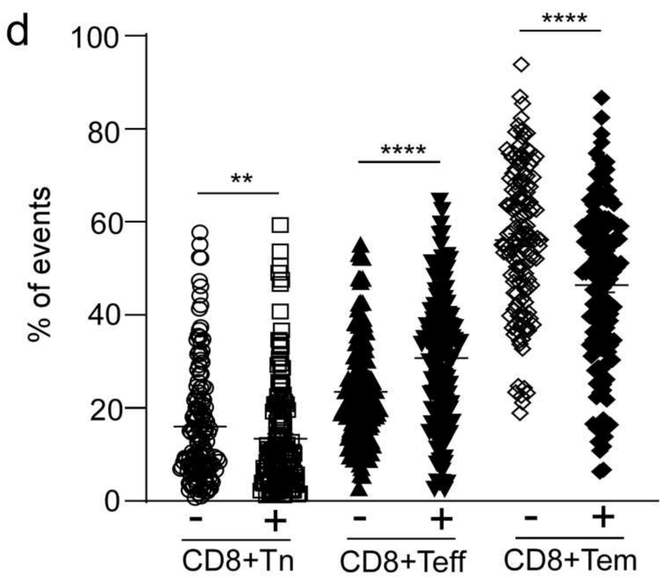
d
****
**
****
% of events
CD8+Tn
CD8+Teff
CD8+Tem

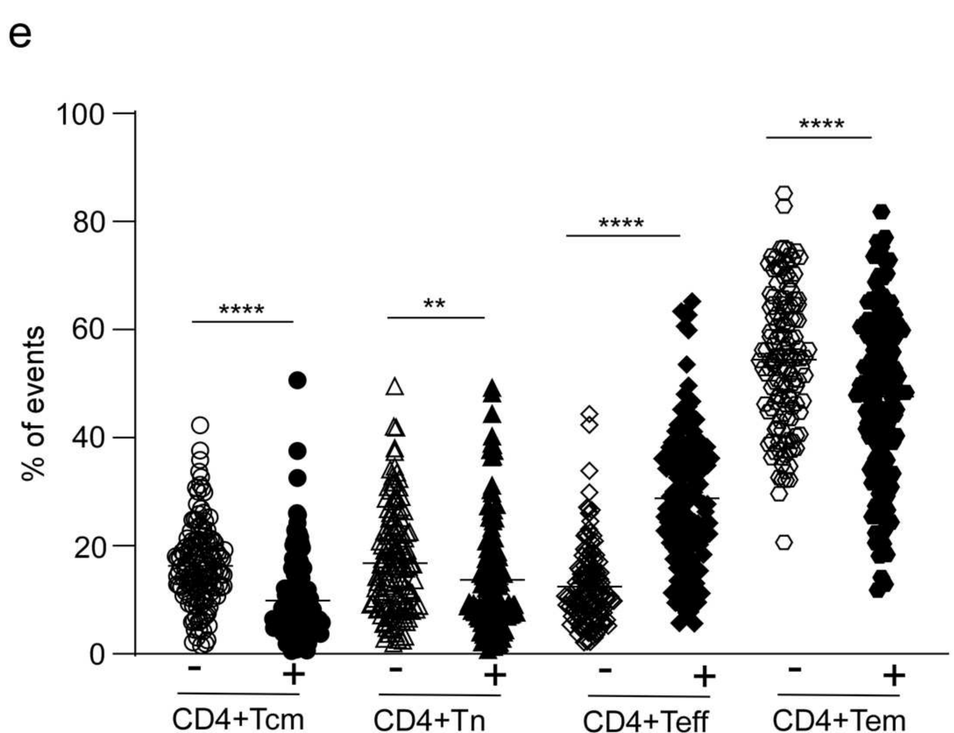
e
****
**
****
****
% of events
CD4+Tcm
CD4+Tn
CD4+Teff
CD4+Tem

Figure 2

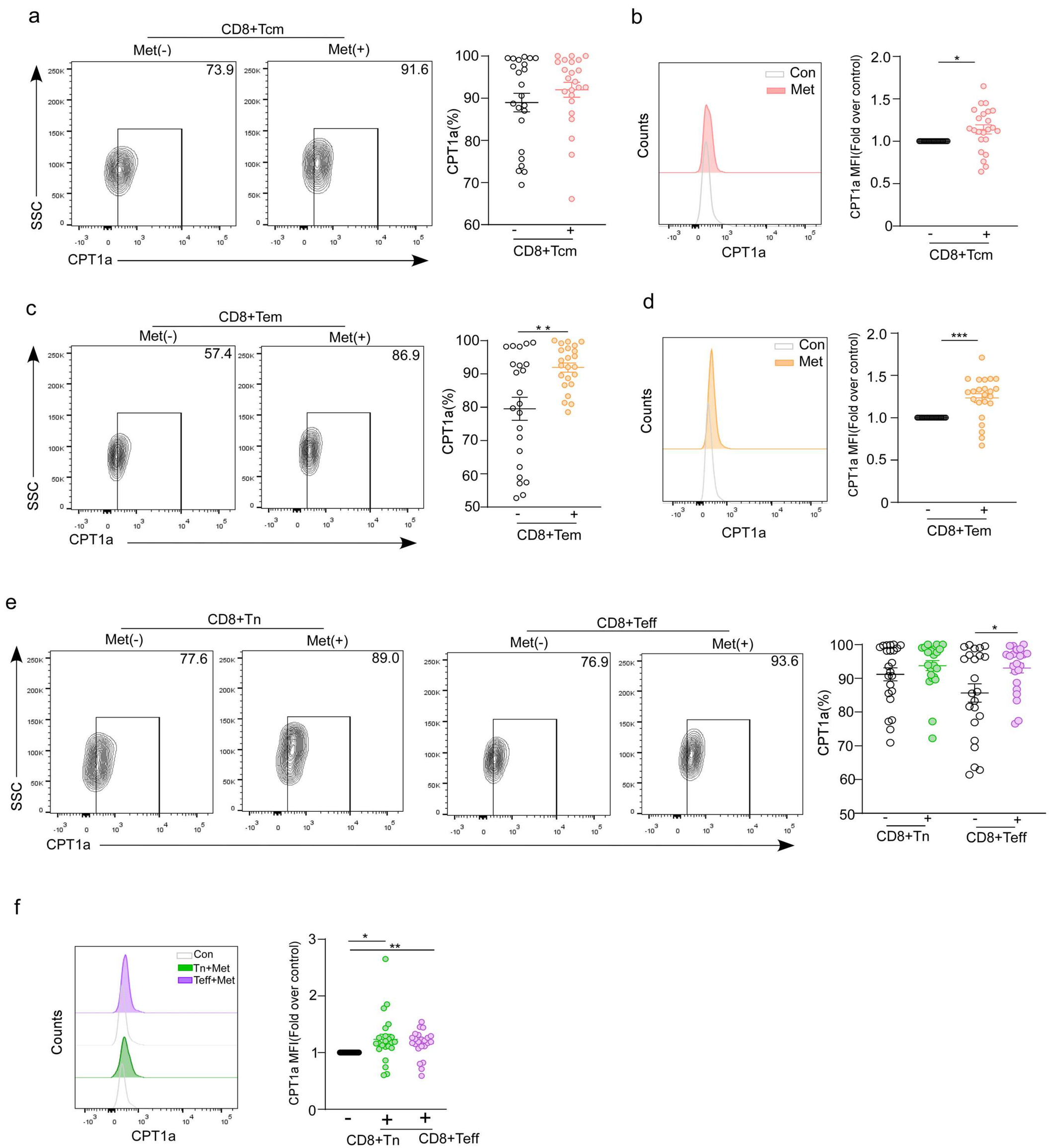
a
CD8+Tcm
Met(-)
Met(+)
73.9
91.6
SSC
CPT1a
CPT1a(%)
CD8+Tcm
b
Con
Met
Counts
CPT1a
CPT1a MFI(Fold over control)
CD8+Tcm
c
CD8+Tem
Met(-)
Met(+)
57.4
86.9
SSC
CPT1a
CPT1a(%)
CD8+Tem
d
Con
Met
Counts
CPT1a
CPT1a MFI(Fold over control)
CD8+Tem
e
CD8+Tn
Met(-)
Met(+)
77.6
89.0
CD8+Teff
76.9
93.6
SSC
CPT1a
CPT1a(%)
CD8+Tn
CD8+Teff
f
Con
Tn+Met
Teff+Met
Counts
CPT1a
CPT1a MFI(Fold over control)
CD8+Tn
CD8+Teff

Figure 3

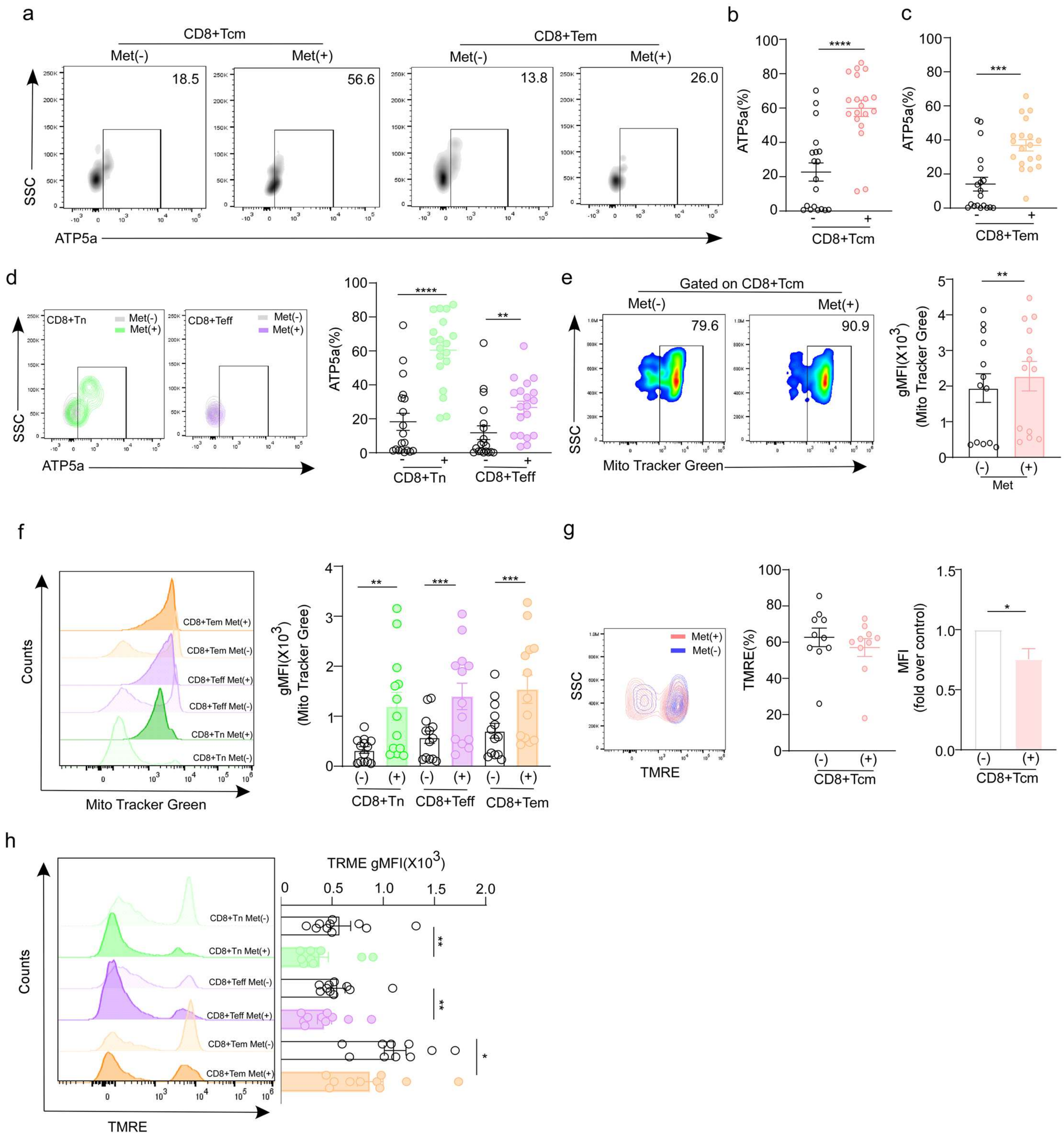
a
CD8+Tcm
Met(-)
Met(+)
18.5
56.6
CD8+Tem
13.8
26.0
SSC
ATP5a
b
ATP5a(%)
****
CD8+Tcm
c
***
CD8+Tem
d
CD8+Tn
Met(-)
Met(+)
CD8+Teff
**
e
Gated on CD8+Tcm
79.6
90.9
Mito Tracker Green
gMFI(X10^3)
(Mito Tracker Gree)
Met
f
Counts
CD8+Tem Met(+)
CD8+Tem Met(-)
CD8+Teff Met(+)
CD8+Teff Met(-)
CD8+Tn Met(+)
CD8+Tn Met(-)
Mito Tracker Green
CD8+Tn
CD8+Teff
CD8+Tem
g
TMRE
TMRE(%)
MFI
(fold over control)
h
TRME gMFI(X10^3)
CD8+Tn Met(-)
CD8+Tn Met(+)
CD8+Teff Met(-)
CD8+Teff Met(+)
CD8+Tem Met(-)
CD8+Tem Met(+)
TMRE

Figure 4

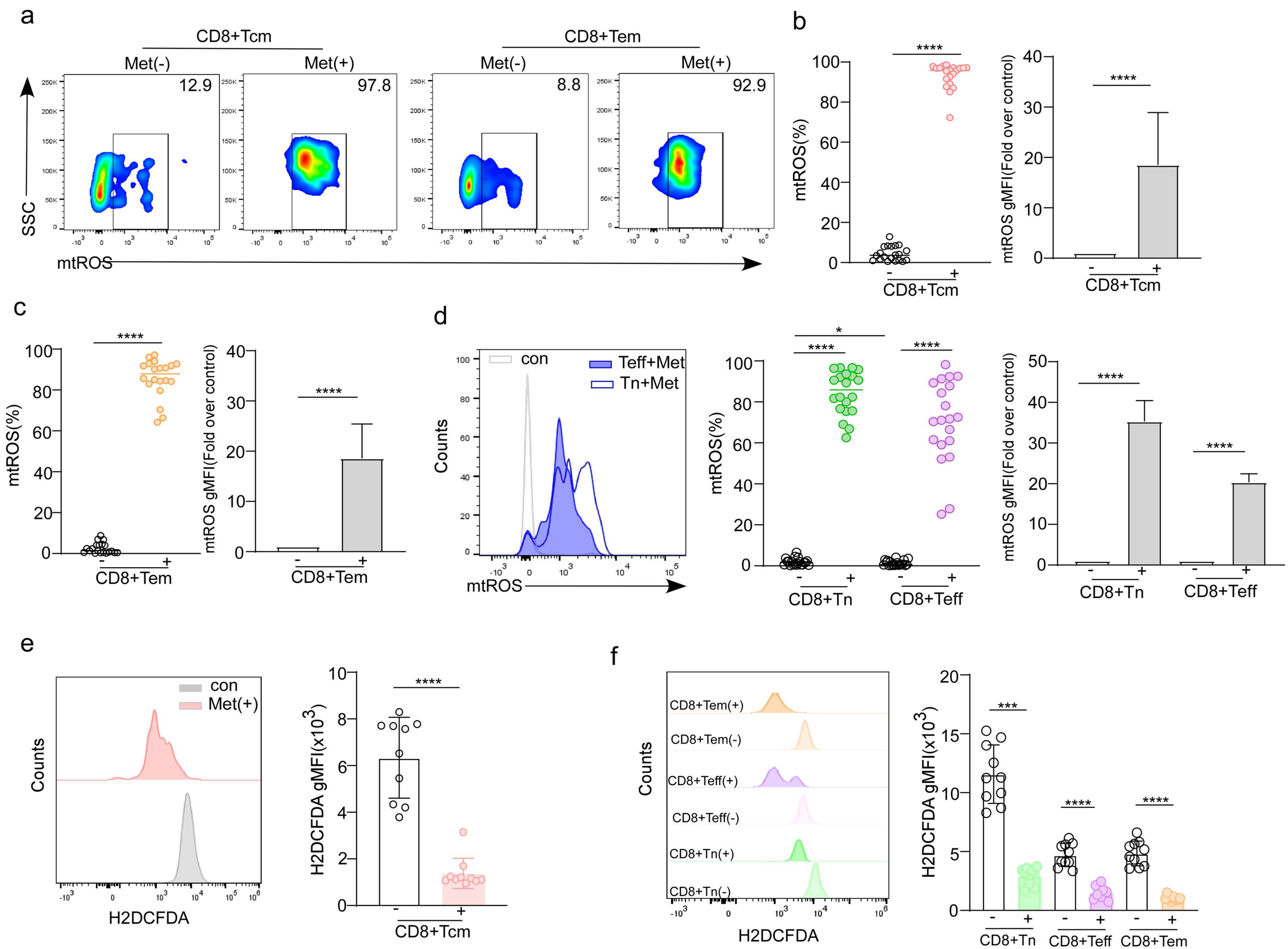
a
CD8+Tcm
CD8+Tem
Met(-)
Met(+)
12.9
97.8
8.8
92.9
SSC
mtROS
b
mtROS(%)
mtROS gMFI(Fold over control)
CD8+Tcm
c
mtROS(%)
mtROS gMFI(Fold over control)
CD8+Tem
d
con
Teff+Met
Tn+Met
Counts
mtROS
CD8+Tn
CD8+Teff
e
con
Met(+)
Counts
H2DCFDA
H2DCFDA gMFI(x10^3)
CD8+Tcm
f
CD8+Tem(+)
CD8+Tem(-)
CD8+Teff(+)
CD8+Teff(-)
CD8+Tn(+)
CD8+Tn(-)
Counts
H2DCFDA
H2DCFDA gMFI(x10^3)
CD8+Tn
CD8+Teff
CD8+Tem

Figure 5

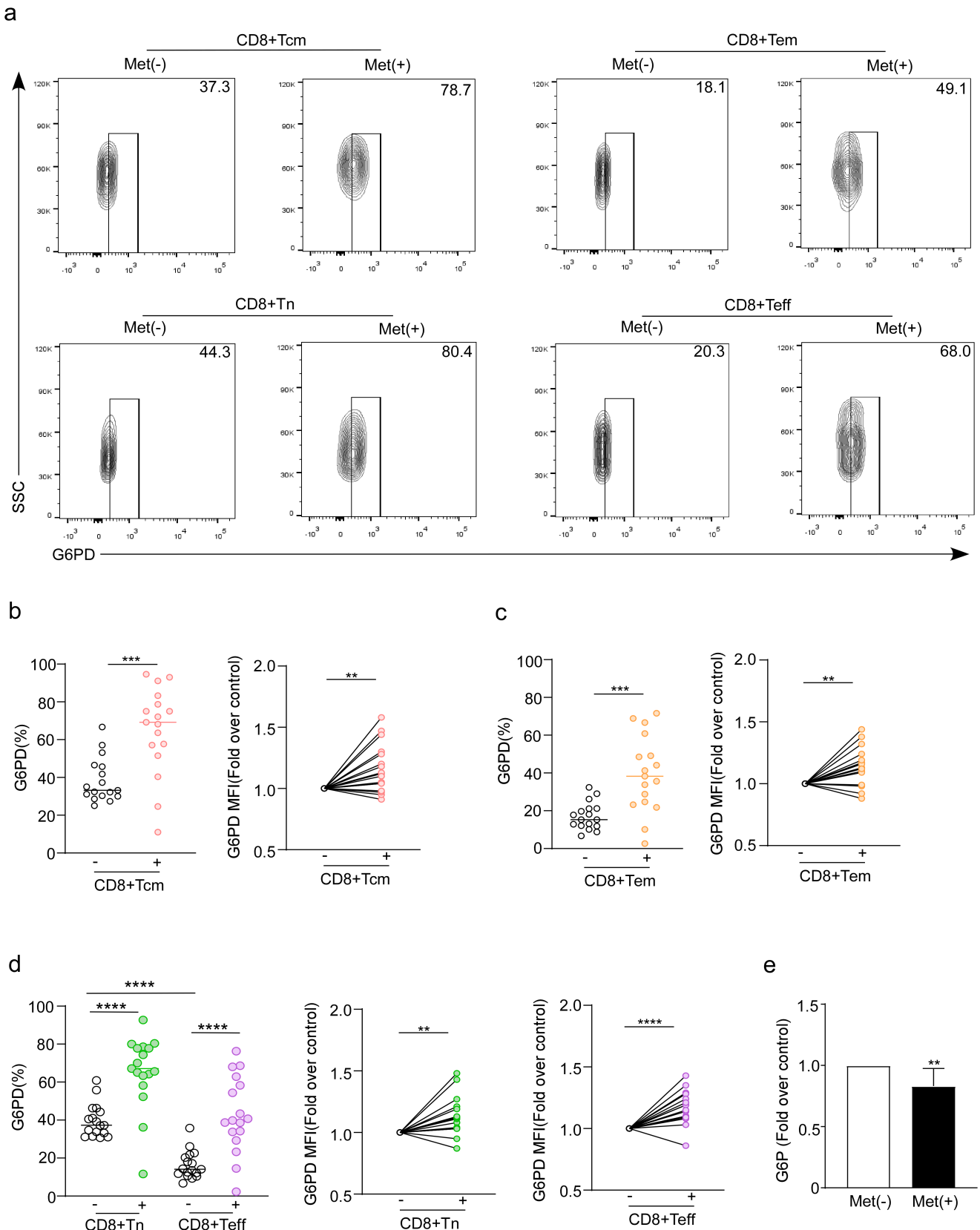
a
CD8+Tcm
Met(-)
Met(+)
37.3
78.7
CD8+Tem
18.1
49.1
CD8+Tn
44.3
80.4
CD8+Teff
20.3
68.0
SSC
G6PD
b
G6PD(%)
G6PD MFI(Fold over control)
CD8+Tcm
c
CD8+Tem
d
CD8+Tn
CD8+Teff
e
G6P (Fold over control)
Met(-)
Met(+)

Figure 6

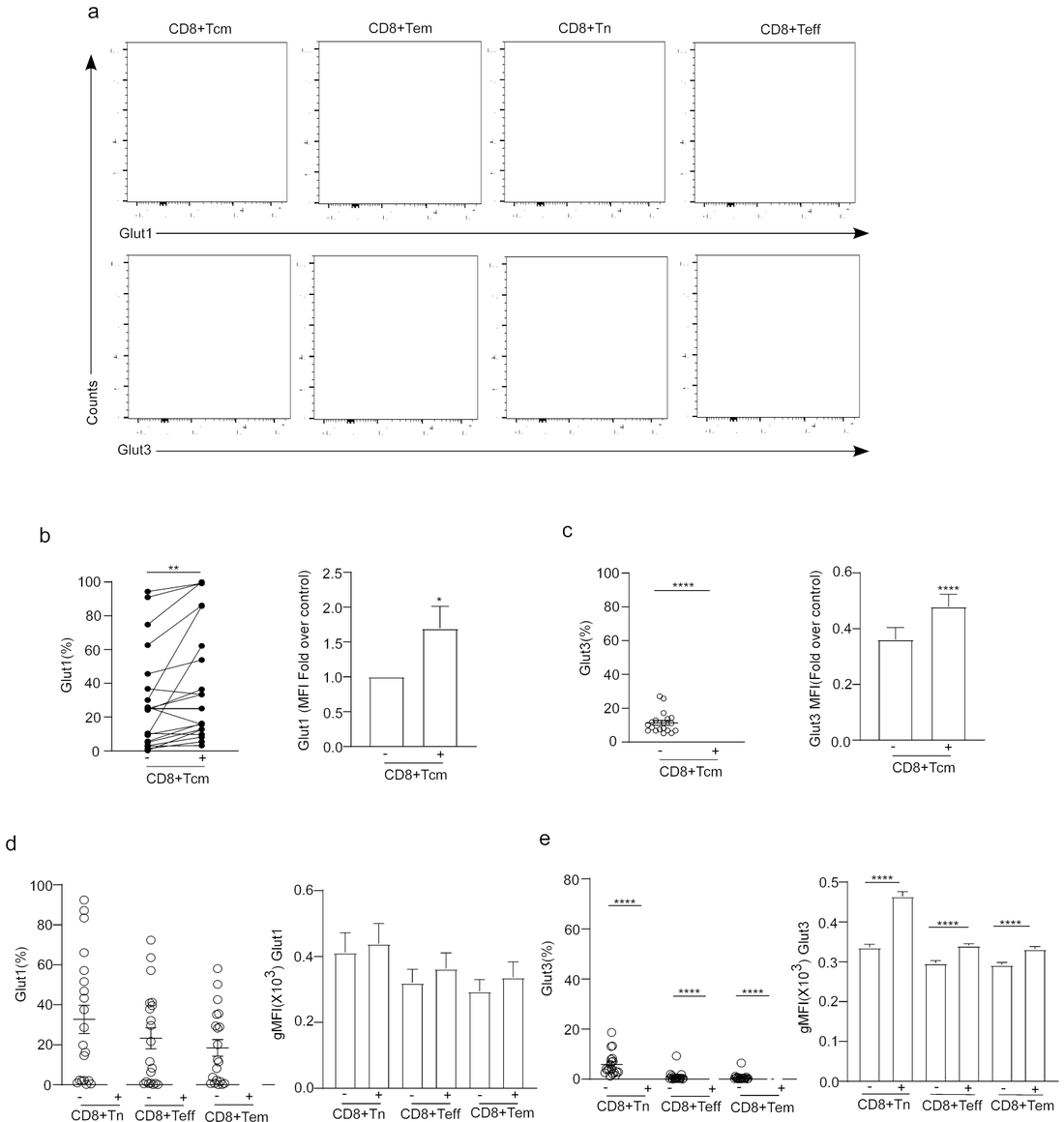
a
CD8+Tcm
CD8+Tem
CD8+Tn
CD8+Teff
Glut1
Counts
Glut3
b
Glut1(%)
CD8+Tcm
Glut1 (MFI Fold over control)
CD8+Tcm
c
Glut3(%)
CD8+Tcm
Glut3 MFI(Fold over control)
CD8+Tcm
d
Glut1(%)
CD8+Tn
CD8+Teff
CD8+Tem
gMFI(X10^3) Glut1
CD8+Tn
CD8+Teff
CD8+Tem
e
Glut3(%)
CD8+Tn
CD8+Teff
CD8+Tem
gMFI(X10^3) Glut3
CD8+Tn
CD8+Teff
CD8+Tem

Figure 7

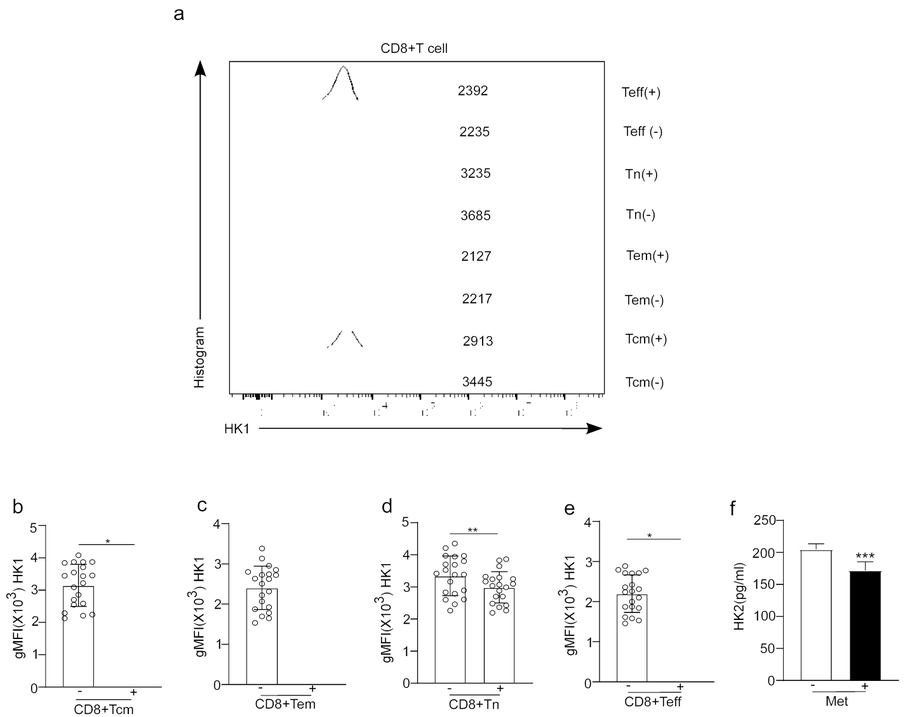
a
CD8+T cell
Histogram
HK1
2392
2235
3235
3685
2127
2217
2913
3445
Teff(+)
Teff (-)
Tn(+)
Tn(-)
Tem(+)
Tem(-)
Tcm(+)
Tcm(-)
b
gMFI(X10^3) HK1
CD8+Tcm
c
gMFI(X10^3) HK1
CD8+Tem
d
gMFI(X10^3) HK1
CD8+Tn
e
gMFI(X10^3) HK1
CD8+Teff
f
HK2(pg/ml)
Met

Figure 8

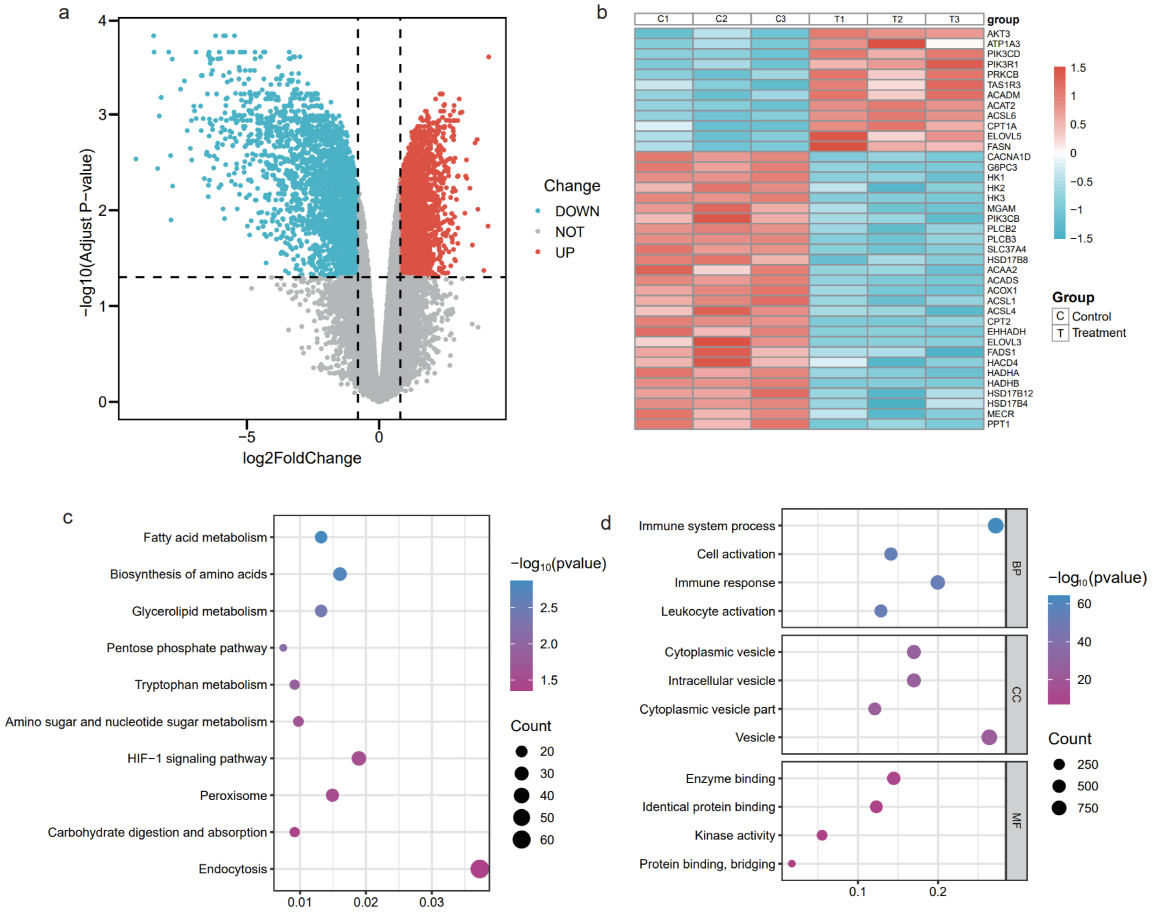
a
−log10(Adjust P−value)
log2FoldChange
Change
DOWN
NOT
UP
b
C1
C2
C3
T1
T2
T3
group
AKT3
ATP1A3
PIK3CD
PIK3R1
PRKCB
TAS1R3
ACADM
ACAT2
ACSL6
CPT1A
ELOVL5
FASN
CACNA1D
G6PC3
HK1
HK2
HK3
MGAM
PIK3CB
PLCB2
PLCB3
SLC37A4
HSD17B8
ACAA2
ACADS
ACOX1
ACSL1
ACSL4
CPT2
EHHADH
ELOVL3
FADS1
HACD4
HADHA
HADHB
HSD17B12
HSD17B4
MECR
PPT1
Group
C Control
T Treatment
c
Fatty acid metabolism
Biosynthesis of amino acids
Glycerolipid metabolism
Pentose phosphate pathway
Tryptophan metabolism
Amino sugar and nucleotide sugar metabolism
HIF−1 signaling pathway
Peroxisome
Carbohydrate digestion and absorption
Endocytosis
−log10(pvalue)
Count
d
Immune system process
Cell activation
Immune response
Leukocyte activation
BP
Cytoplasmic vesicle
Intracellular vesicle
Cytoplasmic vesicle part
Vesicle
CC
Enzyme binding
Identical protein binding
Kinase activity
Protein binding, bridging
MF
−log10(pvalue)
Count

Supplementary Files

This is a list of supplementary files associated with this preprint. Click to download.

- SupFigure1.tif
- SupFigure2.tif
- SupFigure3.tif
- SupFigure4.tif
- SupFigure5.tif